8.1 Overview

8.2 Barrel Region

The pixel detector barrel region (see Figure 1) has three concentric layers with modules loaded on local supports (staves) supported by three shells. The global support described in section 8.1 surrounds the shells and supports them through four radial fingers at the ends of the barrel region. Each stave [1] is about 800 mm

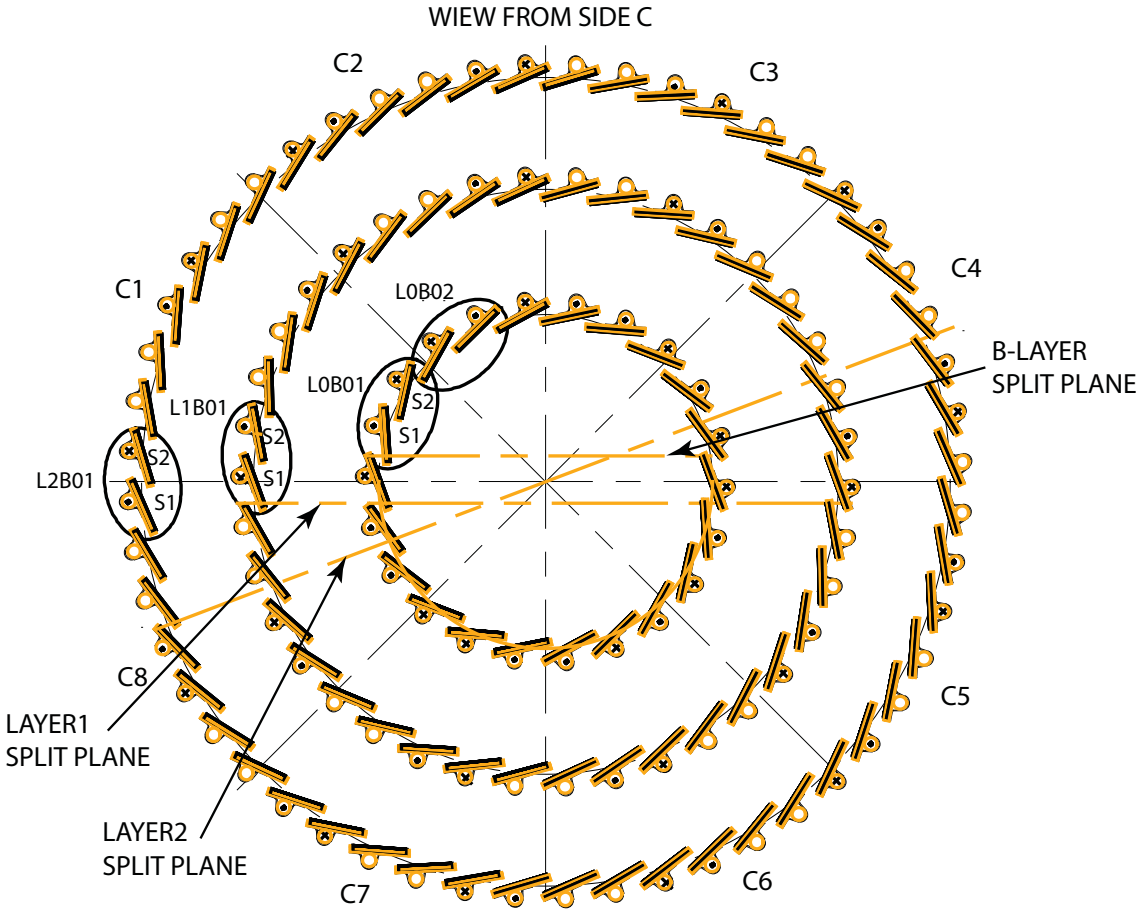

Figure 1: Layout of the Pixel barrel region. Support shells are not shown.

long and carries 13 pixel modules tilted in both the Z-R and R-Φ planes by 1.1° and 20°, respectively. There are in total 112 staves. Two staves share a single cooling loop generating an assembly called a bi-stave with 26 modules. The modules are distributed over the three layers as summarised in Table 1.

	B-layer	Layer 2	Layer 1	Total
Average radius [mm]	50.5	122.5	88.5	
No. of bi-staves	11	26	19	56
No. of staves	22	52	38	112
No. of modules	286	676	494	1456
No. of pixels	$1.317 \cdot 10^7$	$3.115 \cdot 10^7$	$2.276 \cdot 10^7$	$6.709 \cdot 10^7$

Table 1: Parameters of the pixel barrel region.

8.2.1 Staves

A stave is an assembly of three parts (see Figure 2): a Thermal Management Tile (TMT); the omega piece; and the cooling pipe. The TMT is machined out of a

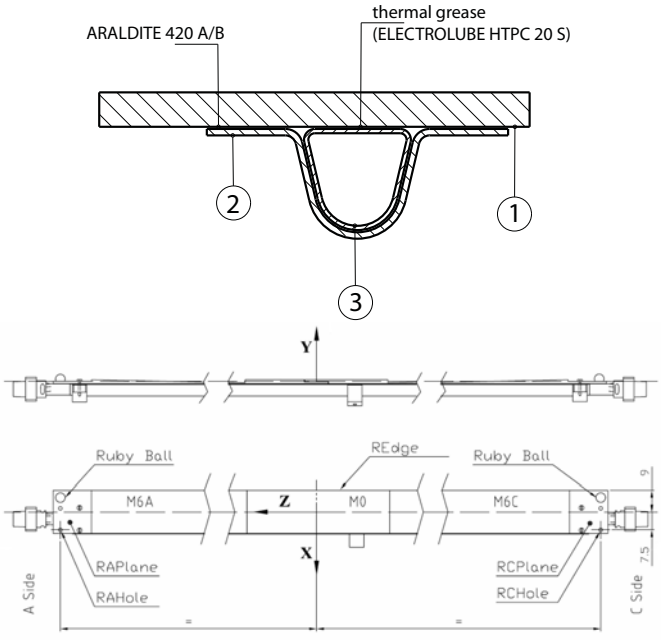

Figure 2: (a) top, cross section of a stave. Part 1 is the TMT, 2 is the omega piece and 3 the aluminum pipe. (b) bottom, longitudinal views of the stave with the reference system used for survey.

Carbon-Carbon (C-C) plate yielding a series of 12 shingled steps symmetrically placed (6 each side) around a central flat step. The shingled geometry allows for an overlap between the 13 modules mounted on the stave, to achieve hermetic coverage. The C-C material has been adopted for many reasons:

- good transverse thermal conductivity, adequate for an efficient heat transfer

from the surface to the cooling channel;

- low radiation length;
- excellent stiffness and stability;
- low value (close to zero) of the coefficient of thermal expansion (CTE).

The omega piece is made of three layers of unidirectional, ultra-high modulus carbon fiber, with cyanate ester resin. The lay-up (0-90-0) is 0.3 mm thick and has been optimized through an extensive design and test program. The choice of the material and of the lay-up has been done in order to achieve a longitudinal CTE as close as possible to the CTE of the C-C TMT, to minimize distortions due to cool down of the structure. The omega-TMT-longitudinal CTE mismatch, less than 1 ppm, allows the stave to meet the stability requirements. The omega is bonded to the TMT using an adhesive[1)] featuring a high peeling strength.

A D-shaped (see part 3 in Figure 2) aluminum pipe, with a 0.3 mm thick wall, is located in the TMT/Omega structure. It provides the cooling channel for the C_3F_8 coolant. The aluminium tube is made of a 6061 Al-alloy, precisely shaped by extrusion to fit inside the omega piece with a clearance of 50 μm. The tube hydraulic diameter is 4.15 mm, which allows cooling of two staves in series with an acceptable pressure drop. A pressure drop of about 50 mbar over one stave has been measured during the thermal tests. Thermal grease[2)] is used to fill the gap between the tube and the TMT. Use of this grease interface reduces the mechanical coupling between the tube and the C-C. This minimizes the stave distortion from cool down.

During the production of staves, several problems were encountered that caused a change in the design and fabrication. The original design had the ends of the aluminium pipe coated with nickel, by an electroless process, in order to attach aluminium fittings by brazing. Staves, before and after modules were loaded, went through a qualification process that used an aqueous solution as a coolant. The presence of water triggered a corrosion process in the aluminium pipes. The corrosion was due to a galvanic process where water and traces of halogen (like Cl) acted as an electrolyte. The effect of the galvanic corrosion led in some cases to holes in the pipe, as may be seen in Figure 3.

A significant number of staves had already been loaded with modules when this problem was found. The solution that was implemented was to insert a new pipe into the existing one. The inserted pipe (see Figure 3) a smaller hydraulic diameter that significantly increased the pressure drop along the pipe. Since the

[1)] CIBA Araldite® 420 A/B, from Huntsman, former Ciba Specialty Chemicals (www.huntsman.com)

[2)] HPGP thermal grease from Electrolube (www.electrolube.com).

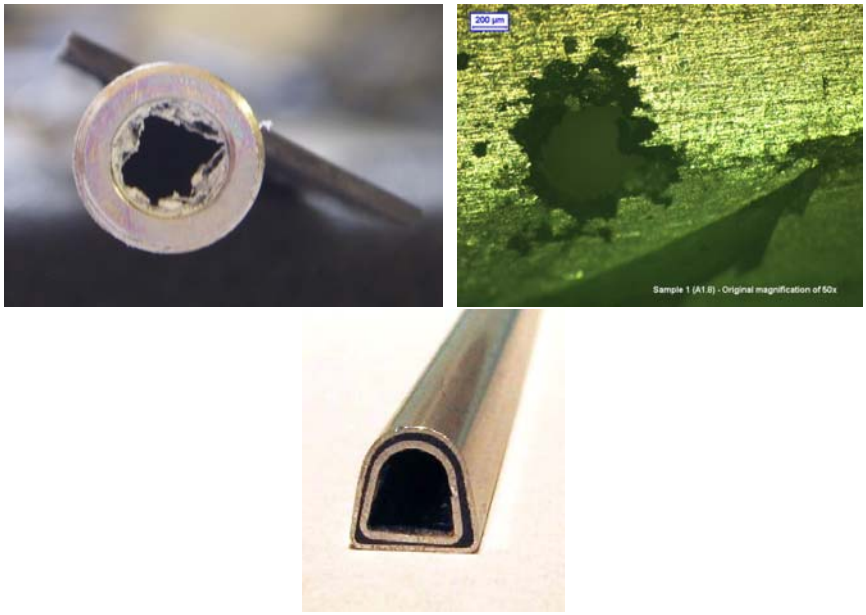

Figure 3: On the left, a view of the end of the stave pipe after corrosion. The nickel layer is detached from the aluminum by the formation of aluminum oxides. The picture in the centre shows a detail of the pipe with a through hole. On the right, a picture of an inserted pipe to recover staves already loaded with modules.

evaporation temperature depends on the pressure, there is a difference in the temperature (ΔT) between the first (higher T) and last (lower T) module of a stave, and this difference was increased for a smaller hydraulic diameter.

The thermal impedance from the coolant to the TMT is also increased for two pipes. There is a 150 μm gap between the two pipes, filled with an alumina loaded epoxy[3)] having a thermal conductivity of 1.1 W/mK. The ΔT increase is $\sim 4^{\circ}$C .

The new pipe was electrically insulated from the original one in order to protect against existing galvanic corrosion at the surface of the external pipe. Hard anodization with an oxide layer of about 30 μm of the inserted pipe was used.

The stave pipe was connected to a cooling system to verify the thermal properties. This connection applied forces to the stave pipe that were transferred to the omega piece, causing delamination the bond between the omega and the TMT. The bond quality was found to be poor because carbon powder from the C-C prevented good adhesion. The bond failure degraded significantly the thermal integrity of the grease layer between the pipe and the TMT. A dedicated inspection performed after the full production showed that more than 5 % of the staves were already delaminated at the fitting area and two of them where already loaded with modules.To prevent further delamination, a glass-filled PEEK collar was added to all the staves that were used in the detector.

The failure modes (corrosion and delamination) led us to develop a recovery plan for the staves already loaded with the modules and for the ones still to be loaded. The recovery plan from corrosion followed three different paths:

1. Insertion of a new aluminium D-shaped pipe into the corroded pipe. Tests performed with an evaporative cooling system have shown that modules of such bi-staves run above 0 °C. Results are reported in Table 2.

2. Fitting were attached to all pipes by laser welding, thereby eliminating eliminating brazing.Bare staves (staves without modules loaded) were disassembled. The old pipe was removed and replaced with one with laser-welded fittings and reassembled with a yield of about 85%.

3. A new batch of staves was produced to compensate for the losses of the refurbished bare staves.

The barrel detector was assembled with a mixture of three different type staves. Table 3 shows how the stave types were assigned to the three layers

8.2.2 Barrel Module Mounting

Modules mounting on staves started in the summer of 2004 to verify procedures. There were three module-loading sites. After qualification of all three sites, pro-

[3)] STYCAST 2850 FT from Emerson & Cuming (www.emersoncuming.com)

Bi-stave type	Stave type	Measured[4)]	
		Mean T	Max T
Repaired Bi-stave	Stave 1 (inserted)	$+3.3^\circ$ C	$+10^\circ$ C
	Stave 2 (clean)	-4.46° C	-0.5° C
Standard Bi-stave	Stave 1	-3.92° C	$+1^\circ$ C
	Stave 2	-5.61° C	0° C

Table 2: Estimated and measured temperature for different bi-staves. Stave 1 is upstream and Stave 2 is downstream in the cooling loop.

Type	Comments	Layer 2	Layer 1	B-Layer	Total
Inserted staves Pipe inserted (1)	26	0	0	26	
New Staves New pipes (2)	2	15	11	28	
Repaired Staves Pipe substituted (3)	24	23	11	58	

Table 3: Distribution of the different types of staves in the barrel layers.

duction continued at full speed until the corroded aluminum pipes in staves were discovered. This problem stopped module loading for six months. Once new staves were available, module loading was immediately restarted and later continued in parallel with bare stave production. The last stave was assembled in October 2007.

The loading procedure and the qualification tests are described in the following paragraphs. Stave loading was done using specially designed robots in a semi-automatic way by trained operators. Three module loading robots were installed: sites 1 and 2 had similar designs (shown in Figure 4), while site 3 had a different one [2]. All setups were located in clean rooms with temperature control.

Detector modules had to be fixed with a precision better than 50 μm in both directions on the stave plane. Nominal module positions were defined in a stave reference coordinate system constructed individually for each stave based on stave reference points (machined edges, tile steps and reference planes on stave ends). Some of these reference points are inaccessible after stave loading, so to control the module positions and to translate these positions to the global ATLAS coordinate frame, two precision ruby balls were mounted on each stave. Together with the reference planes, they allow the measurement of module positions.

The determination of the stave reference frame and the survey of module positions after stave loading was done with a coordinate measuring machine (CMM) with mechanical, optical and laser probes at sites 1 and 2. Site 3 used a specially designed optical system connected with the loading robot. The single point measurement precision was between 5 and 10 μm for contact probes and between 5 and 20 μm for optical probes depending on the surface quality. Several measured

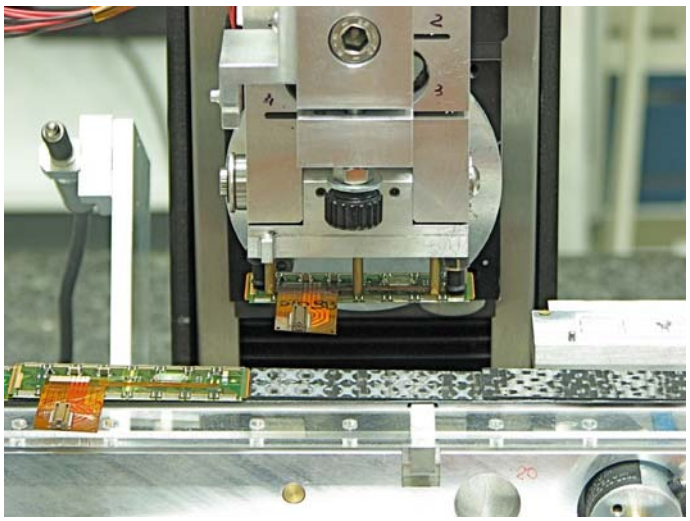

Figure 4: Loading robot used in sites 1 and 2. Blow up of the module pick-up head.

points were averaged to improve accuracy.

Loading started with a determination of the stave reference system. The stave was fixed on a moving trolley (sites 1 and 2) or granite table (site 3) to guarantee precise placement of the modules by the loading robot. To guarantee uniform cooling, a gap between a pixel module and the stave surface must be constant ($\sim$100 μm) everywhere. Due to the shingled-stave design, modules are inclined by $\sim$1.10° before gluing. The ideal position of a pixel module located 100 μm above the stave surface was stored in the robot memory and module was moved away to allow glue deposition.

A thermal-conducting, flexible epoxy glue [5)] was used to fix modules. After glue deposition, a module was returned by the robot to its predefined position 100 μm above stave surface and left in this position until the glue cured. The force holding the module was adjusted to control the quality of module-stave joint.

A loaded stave was surveyed on a CMM. Deformation of pixel modules (bow) was measured using different methods. All measurements were taken with respect to the two ruby balls mounted on each stave. The deviation of modules position from nominal in X (transverse to the stave axis) and Z (along the stave axis) co-ordinates are shown in Figure 5 [3]. Only a few modules have deviations bigger than 50 μm.

The fully-loaded staves under to measure a characterization procedure to test the modules after the loading as well as to measure the thermal performance of

[5)] Toray Silicone SE4445CV A&B, from Dow Corning (www.dowcorning.com)

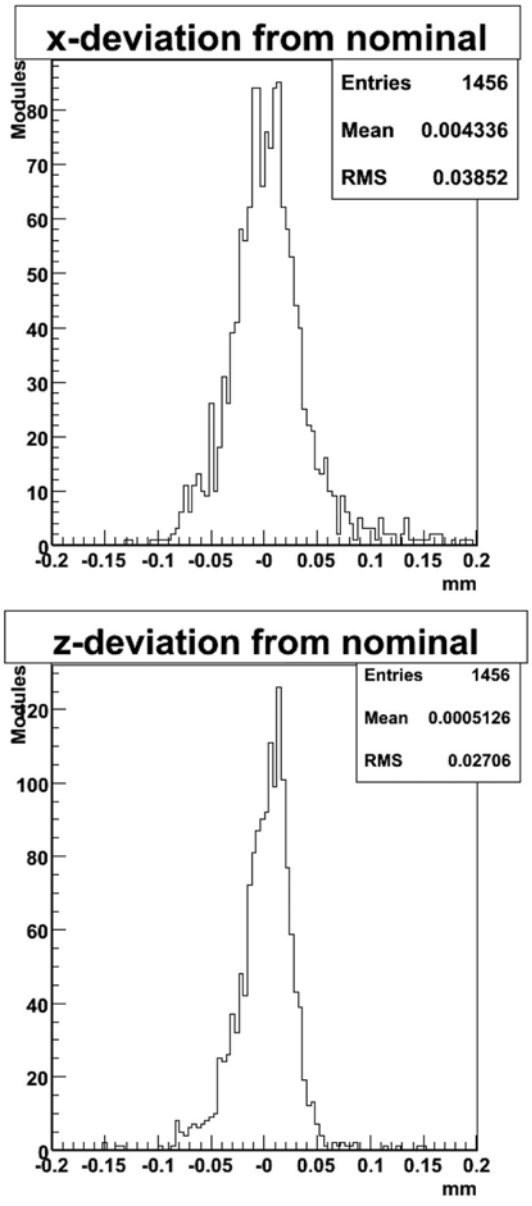

Figure 5: Deviation of module positions from nominal values for the barrel modules as described in the text.

the assembly. The testing sequence was similar to the one used to qualify modules individually. The testing sequence was as follows:

- module configuration, measurement of threshold dispersion and noise, threshold scan without bias to check for disconnected pixels and a sensor bias I-V scan to check the integrity of the sensor at room temperature;
- ten thermal cycles between -30°C and 30°C with a cycle time of 2 hours;
- the same tests as performed at room temperature but at about -8°C with the addition of a radioactive-source scan for the identification of disconnected pixels. The thermal performance was also obtained.

A ranking function of the measured parameters was constructed to determine the stave quality and to select the staves for a particular layer. The best staves went into the B-layer. Staves with an inserted pipe were only used in Layer 2 (Table 2).

8.2.3 Half-shells

The barrel shells (see Figure 6) were constructed from two half-shells. Bi-staves were attached to a half-shell. Ten aluminium-alloy fasteners screw each bi-stave to support rings bonded to a shell. All the shells are supported off the end-cones of the pixel support frame (Section 8.l) PEEK elements are bonded at both ends of the half-shell to provide the interface to the fingers of the end-cones. Shells

Figure 6: Picture of the three barrel shells

were made from carbon-fiber-reinforced material. A quasi-isotropic laminate made of six plies $(0^\circ/60^\circ/-60^\circ)$ of unidirectional ultra-high-modulus carbon

fiber[6]/cyanate-ester[7] was made. The shells are not cylinders, but have flat surfaces locally. The overall mass was reduced by cutting out material in each shell, as show in Figure 6.

The accuracy of the interface to a stave was set to be better than 50 μm. The maximum gravity deflection of each assembly was designed to be less than 50 μm. Table 4 shows results from a survey done on the as-built assembly. The values

	Shell Accuracy [μm]			
	Requirements	As built		
	All Layers	Layer 2	Layer 1	B-Layer
Geometrical accuracy	50	70	62	55
Gravity sag	50	98	68	80

Table 4: Comparison between the geometrical design requirements and the maximum deviations from an ideal geometry as surveyed.

reported in the table are the maximum deviations observed over several hundred data points taken all over the structures. The large majority of them ($> 90\%$) are within the specifications.

8.2.4 Bi-stave Integration and Half-shell Loading

Two staves (see Figure 7), each loaded with 13 pixel modules, were assembled together. Type 0 cables (section 8.5) were connected to the module and properly routed along the staves. Electrical testing was done during bi-stave assembly as was leak checking of the two cooling loops after connection of a U-link (section 8.5)

Bi-staves were integrated by hand into the half-shells starting with Layer 2 and proceeding to the B-Layer. Figure 8 shows one of two half-shells with all the bi-staves installed for Layer 2.

Once the bi-stave loading was completed, the half-shells underwent a geometrical survey. The stave reference points provided by two ruby balls glued at the ends of each stave were surveyed with respect to the half-shell reference points. Although the module position is known in Z with a typical accuracy of about 10 μm, the inaccuracy in Φ and in R is significantly worse. The stave can bow in a half-shell during attachment up to 200 μm in Φ at the central support (Z=0). The effects on individual modules could not be determined because modules could not be surveyed directly on a half-shell.

[6] Carbon fiber YS80, from Nippon Graphite Fiber Corporation (NGF) (http://www31.ocn.ne.jp/ ngf/english/)

[7] EX-1515 Cyanate Ester resin system, from TenCate Advanced Composites, former Bryte Technologies Inc (www.brytetech.com)

Figure 7: A bi-stave assembly.

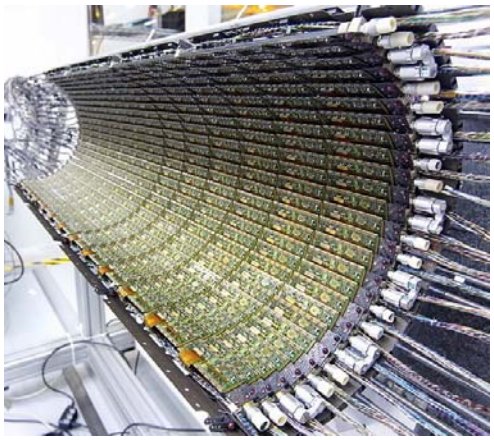

Figure 8: Layer 2 half-shells with all the bi-staves installed.

8.2.5 Half-shell Clamping

Two half-shells of each layer were clamped together into a complete shell. A half-shell lacks torsional stiffness (around the axis of the cylinder). Half-shells were stiffened with an external structure and kept undeformed during the integration process. The shell transferring tool (STT) held each of the two half-shells by ten clamps that grabbed each half-ring in two places. The tool was placed on the flat surface of a granite table that provided the reference plane. The bottom half-shell is kept on the STT and the top one was lowered until it engaged the clamping features (see Figure 9).

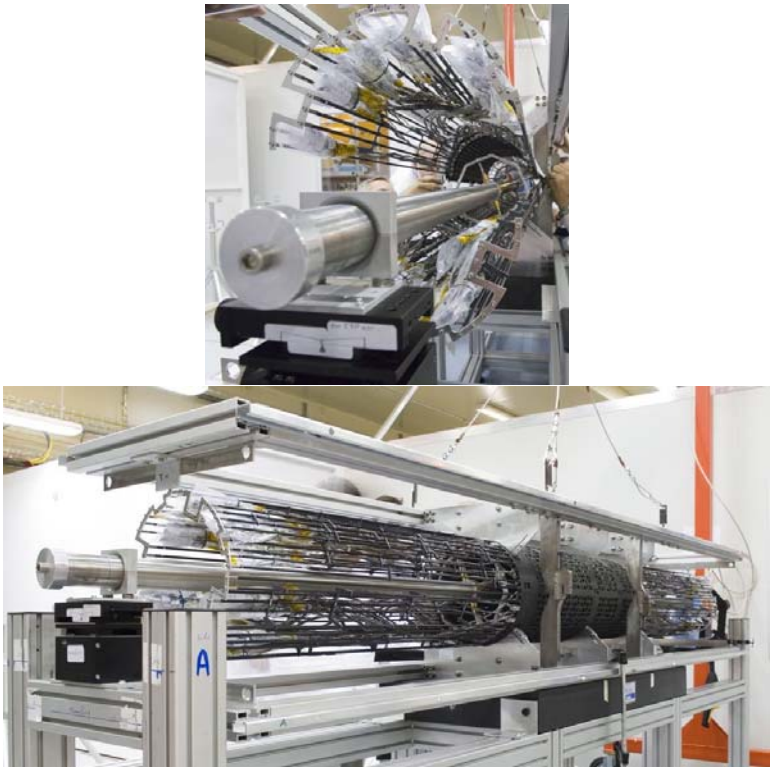

Figure 9: Clamping of the Layer 2 half-shells. The top half is craned onto the bottom one resting on the STT (see text). The picture shows the mechanism that guides the process. The stainless steel pipe, visible along the the axis of the shell, was used to guide the insertion into the global frame and was removed afterward.

The operation was delicate due to the fact that the wire bonds of the modules were exposed and clearances were about 1mm. Once the half-shells are joined, they can be removed from the STT. The load of the shell was taken by the metal

pipe passing through the shell and visible in Figure 9. Figure 10 shows the Layer 2 shell clamped and moved onto the integration and testing tool (ITT) for integration into the global support frame (section 8.6). Layer 1 followed the same clamping

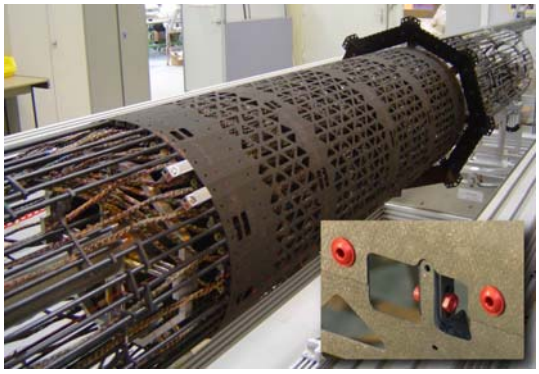

Figure 10: Layer 2 clamped and resting on the axis of the ITT before being inserted into the global frame.

procedure. The B-layer required a more complex procedure. The flanges at the extremities of the beam pipe do not pass through the B-Layer and it has to be clamped around them (Section 8.6). More details of the assembly and testing procedures can be found in [4].

References

[1] M. Olcese, C. Caso, G. Castiglioni, R. Cereseto, S. Cuneo, M. Dameri, C. Gemme, K. W. Glitza, G. Lenzen, and F. Mora. Ultra-light and stable composite structure to support and cool the atlas pixel detector barrel electronics modules. *Nucl. Instr. and Meth. A*, 518(3):728–737, 2004.

[2] Karl-Heinz Becks, Peter Gerlach, Karl-Walter Glitza, Pascal Knebel, Peter Mattig, Bernd Sanny, Sebastian Reuschel, Swetlana Springer, and Bernd Witt. Local support assembly of the atlas pixel detector. *Nucl. Instr. and Meth. A*, 565(1):102–105, 2006.

[3] A. Andreazza, V. Kostyukhin, and Madaras. R. Survey of the atlas pixel detector components. ATL-IP-QC-0035, CERN, Sept. 2006.

[4] E. Andersen, K. Einsweiler, D. Giugni, C. Glitza, G. Lenzen, N. Hartman, M. Garcia-Sciveres, M. Gilchriese, M. Olcese, L. Rossi, B. Sanny, E. Vigeolas, and S. Coelli. Atlas pixel detector assembly and testing of the pixel detector system. ATL-IP-QA-0007, CERN, October 2007.